Dynamic Fluid Connectivity Controls Solute Dispersion in Multiphase Porous Media Flow

Joachim Mathiesen, Gaute Linga, Marek Misztal, François Renard, Tanguy Le Borgne

Geophysical Research Letters

RESEARCH LETTER
10.1029/2023GL105233

Dynamic Fluid Connectivity Controls Solute Dispersion in Multiphase Porous Media Flow

Joachim Mathiesen[1,2], Gaute Linga[2], Marek Misztal[1], François Renard[2,3], and Tanguy Le Borgne[2,4]

[1]Niels Bohr Institute, University of Copenhagen, Copenhagen, Denmark, [2]The Njord Centre, Departments of Geosciences and Physics, University of Oslo, Oslo, Norway, [3]ISTerre, University Grenoble Alpes, Grenoble INP, University Savoie Mont Blanc, CNRS, IRD, University Gustave Eiffel, Grenoble, France, [4]CNRS, Géosciences Rennes, University Rennes, UMR 6118, Rennes, France

Key Points:

- Solute dispersion in multiphase flow is significantly amplified by dynamic fluid connectivity
- We derive a scaling law for the solute dispersion in multiphase systems applicable to a wide range of subsurface geosystems
- We propose a phase diagram for the dispersion coefficient in terms of Capillary and Péclet numbers

Supporting Information:

Supporting Information may be found in the online version of this article.

Correspondence to:

J. Mathiesen,
mathies@nbi.ku.dk

Citation:

Mathiesen, J., Linga, G., Misztal, M., Renard, F., & Le Borgne, T. (2023). Dynamic fluid connectivity controls solute dispersion in multiphase porous media flow. *Geophysical Research Letters*, *50*, e2023GL105233. https://doi.org/10.1029/2023GL105233

Received 28 JUN 2023
Accepted 28 JUL 2023

Author Contributions:

Conceptualization: Joachim Mathiesen, Gaute Linga, François Renard, Tanguy Le Borgne
Formal analysis: Joachim Mathiesen, François Renard, Tanguy Le Borgne
Funding acquisition: François Renard
Methodology: Joachim Mathiesen, Gaute Linga, Marek Misztal, François Renard, Tanguy Le Borgne
Project Administration: Joachim Mathiesen, François Renard, Tanguy Le Borgne
Software: Joachim Mathiesen, Gaute Linga, Marek Misztal
Visualization: Joachim Mathiesen

Abstract Solute transport in multiphase flow through porous media plays a central role in many natural systems and geoengineering applications. The interplay between fluid flow and capillary forces leads to transient flow dynamics and phase distributions. However, it is not known how such dynamic flow affects the dispersion of transported species. Here, we use highly resolved numerical simulations of immiscible two-phase flow to investigate dispersion in multiphase flows. We show that repeated activation and deactivation of different flow pathways under the effect of capillary forces accelerates the spreading of solutes compared to single phase flow. We establish the transport laws under dynamic multiphase flows by linking the dispersion coefficient to the Bond number, the ratio of the force driving the flow and the surface tension. Our results determine the controlling factors for solute dispersion in porous media, opening a range of applications for understanding and controlling transport in porous geological systems.

Plain Language Summary When a single fluid flows through porous media such as soils or geological reservoirs, the transport of contaminants, nutrients, microorganisms, and chemicals is fairly well understood. When two or more fluids flow together, these transport phenomena have largely not been considered despite their importance in many natural systems. Forces between the flowing fluids and the solid boundaries may create large variations in the local flow rates and form time-varying flow pathways, which can in turn accelerate solute spreading. Here, we use extensive computer simulations of flow to suggest a new theory for how solute spread in systems of two fluids flowing through porous media which may help us understand and control transport properties in natural systems.

1. Introduction

The dispersion and mixing of elements transported by fluids in porous media are key processes controlling the fate and transformation of contaminants, nutrients, microorganisms, chemicals, and gases in numerous natural and engineered systems in the subsurface (Bochet et al., 2020; Chen et al., 2017; De Gennes, 1983; Hartmann et al., 2021; Harvey et al., 2002; Kirchner et al., 2000; Osselin et al., 2022; Rolle & Le Borgne, 2019; Szulczewski et al., 2012). Under fluid-saturated conditions, models, and theories that relate the dispersion properties to the porous media structure and heterogeneity are well established (Berkowitz et al., 2006; Bijeljic et al., 2011; Bordoloi et al., 2022; De Anna et al., 2013; Dentz et al., 2011; Kang et al., 2014; Le Borgne et al., 2008; Meigel et al., 2022; Neuman & Tartakovsky, 2009; Puyguiraud et al., 2021). However, in many porous systems, several fluid phases, including water, gas, and different immiscible fluids, coexist in the pore space (Blunt, 2017; Holtzman et al., 2020; Zhao et al., 2016). Dispersion in such multiphase flows affects several important processes, including contaminant and nutrient transport in soils and catchments (e.g., Kirchner et al., 2000; Sebilo et al., 2013), brine and nutrient transport in snow and sea ice (e.g., Golden, 2001; Waldner et al., 2004), CO_2 sequestration in geological reservoirs (e.g., Szulczewski et al., 2012; Zheng et al., 2017), underground hydrogen storage (Lysyy et al., 2022; Tarkowski, 2019), and solute dispersion in gas seepage sites (e.g., Aiken et al., 2022; Scandella et al., 2016).

The increase of computational power and imaging capabilities allow to explicitly resolve flow and transport over an increasing range of scales (e.g., Yeh et al., 2023). However, for highly non-linear processes, such as multiphase flow, current numerical methods can resolve the transient pore scale flow over tens to hundreds of grains at most

Writing – original draft: Joachim Mathiesen, Gaute Linga, François Renard, Tanguy Le Borgne
Writing – review & editing: Joachim Mathiesen, Gaute Linga, Marek Misztal, François Renard, Tanguy Le Borgne

(e.g., Ferrari et al., 2015). Therefore, it remains an important task to derive effective transport parameters quantifying unresolved subscale processes.

The control of multiphase flow properties on transport dynamics has been debated in the last two decades (Bromly & Hinz, 2004; Harter & Yeh, 1996; Hasan et al., 2020; Jiménez-Martínez et al., 2015, 2017; Nützmann et al., 2002; Padilla et al., 1999; Triadis et al., 2019; Vanderborght & Vereecken, 2007; Velásquez-Parra et al., 2022). Consistently with stochastic transport theories (e.g., Dentz et al., 2011), the general trend is that dispersion is larger in unsaturated flows compared to saturated flows due to an increase in flow heterogeneity. However, there is currently no quantitative model able to predict this phenomenon from the basic non-dimensional parameters that describe multiphase flow dynamics. Recent work on dispersion in multiphase flows has focused on the particular case where the distribution of fluid phases is "frozen" in time (Jiménez-Martínez et al., 2015, 2017; Velásquez-Parra et al., 2022). The fixed distribution typically occurs after a transient regime when a non-wetting fluid remains trapped by capillary forces. This requires that the pressure difference at the interface of the two phases is everywhere below the capillary threshold.

In many multiphase flow systems this condition is not fulfilled, resulting in a highly intermittent flow field (Gao et al., 2020; Reynolds et al., 2017; Rücker et al., 2015). The intermittent flow is characterized by large-scale avalanches in the mobility of the fluid phases (Dougherty & Carle, 1998; Planet et al., 2009; Primkulov et al., 2022; Tallakstad et al., 2009a; Zhao et al., 2016), which fundamentally modify the transport dynamics compared to single-phase and frozen multiphase flows. Yet, how the nature of multiphase flow influences solute dispersion remains unknown. Intermittent flows are well-established in co-flow systems, where two phases flow simultaneously under a globally steady-state flow (Datta et al., 2014; Reynolds et al., 2017; Tallakstad et al., 2009a). Co-flow results in dynamic connectivity (persistent fluctuations) of flow pathways under a large range of flow rates and saturations (Datta et al., 2014; Gao et al., 2021).

Here, we use numerical simulations in two and three dimensions under co-flow conditions to establish how dynamic multiphase flow controls solute dispersion in a wide range of multiphase flow systems in the subsurface. We explore a large range of Capillary and Péclet numbers. The Capillary number characterizes the relative effect of viscous drag versus surface tension γ, $\mathrm{Ca} \equiv \mu_w \langle v \rangle / \gamma$ where μ_w is the dynamic viscosity of the wetting fluid and $\langle v \rangle$ the average flow speed. The Péclet number characterizes the relative effect of advection and diffusion, $\mathrm{Pe} \equiv \ell \langle v \rangle / D_m$, where ℓ is a characteristic length scale (given by the pore scale) and D_m is the molecular diffusion constant.

While solute dispersion along the primary flow direction (longitudinal dispersion) is controlled mainly by the solid structure, transverse dispersion becomes strongly enhanced relative to single phase flow when the Péclet number is larger than unity. This is a consequence of dynamic fluid connectivity, where local pathways are constantly reorganized by the movement of the boundaries between the fluid phases (Figure 1). We demonstrate that the relevant scale driving this enhanced dispersion follows from a non-linear function of the ratio between the surface tension and the body force driving the flow. We thus establish the laws of dispersion in dynamic multiphase porous media flows, as a function of both Capillary and Péclet numbers.

2. Methods

Based on the free-energy Lattice Boltzmann Method (Connington & Lee, 2013), we perform simulations in two systems, a two-dimensional (2D) cell of size $L_\perp \times L_\parallel = 2{,}048 \times 768$ filled with non-overlapping cylindrical obstacles, radius $r = 8$ and a three-dimensional (3D) cell of size $L_{\perp,1} \times L_\parallel \times L_{\perp,2} = 256 \times 384 \times 256$ filled with overlapping spheres, radius $r = 8$. All lengths are here given in lattice units. The porosity is measured as the fraction of area/volume not covered by cylinders/spheres and is 53% in 2D and 21% in 3D. Note that the porosity of the 2D cell is large compared to natural porous media, which is needed in 2D for good connectivity (De Anna et al., 2013). See Text S1 and Figure S1 in Supporting Information S1 for a description of how we generate the porous systems and for a description of how our dimensionless simulation parameters can be converted to real parameters. The SI also contains information about our numerical code available at Ref. (Mathiesen et al., 2023). Movies S1 and S2 present movies of two- and three-dimensional simulations.

The two fluid phases have a kinematic viscosity ratio $\nu_w/\nu_{nw} = 0.57$ and a density ratio $\rho_w/\rho_{nw} = 1.25$ equivalent to a system filled with water and silicone oil. The density difference is not significantly influencing the flow and, in the considered regime, both phases are mobilized (Text S1 and Figure S3 in Supporting Information S1,

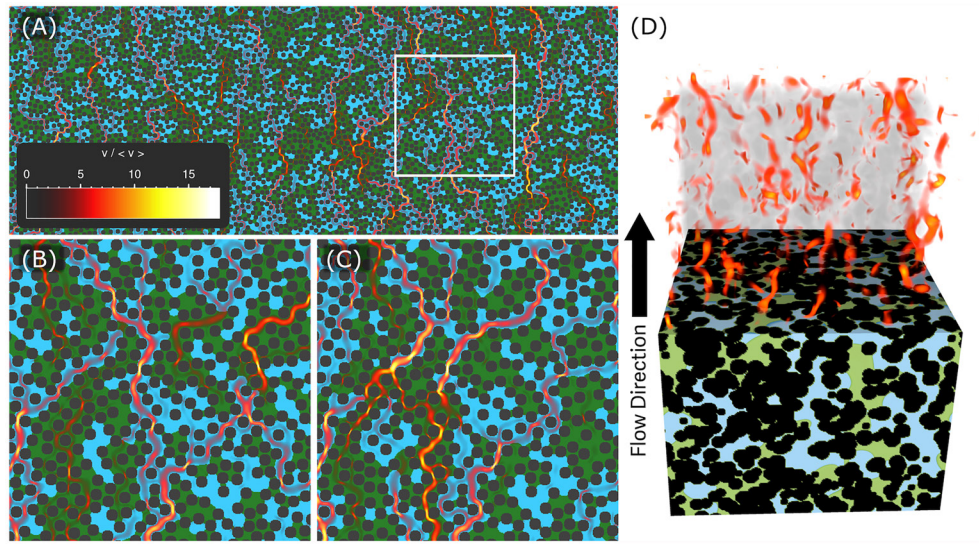

Figure 1. Simulations of the flow of two immiscible fluids in a porous medium (Bo = 0.18). The flow is driven by a body force pointing in the direction of the shown arrow from the bottom to the top. The non-wetting (green) and wetting (blue) fluids flow between fixed cylindrical obstacles (black circles) forming the porous medium. The local fluid velocities are indicated by red to white colors overlaying the fluid phases. For two-dimensional simulations, panel (a) shows the full system and panels (b, c) show zooms inside the white box of panel (a) for two different time steps. Overall the flow is highly heterogeneous and dynamic, as illustrated by the temporal variations in the flow pathways between the panels (b, c). Panel (d) shows a corresponding figure for the three-dimensional system.

we present results from a system with two fluids of equal density and viscosity). The wetting angle is imposed to be 60° and the non-dimensionalized surface tension γ is varied in the interval [0.005, 0.040]. In addition to the multiphase simulations, we have computed the corresponding single-phase flow field satisfying the Stokes equations. All simulations are initiated in a state where the two phases are arranged in alternating stripes of width $2r$ transverse to the main flow direction. Following (Ramstad et al., 2012), we drive the flow by a body force density $\rho_{w/nw}\mathbf{g}$ pointing along $L_{\|}$. Our system has periodic boundary conditions in all directions, that is, when a fluid phase exits on one side, it reenters on the opposite side of the cell. In this way we avoid capillary end-effects.

We initialize the system with $N = 15{,}000$ passive point particles initially uniformly distributed through the system. Particles move by both advection and diffusion. Their trajectories $\mathbf{x}_i(t)$ are found by numerically solving the stochastic differential equation

$$\frac{d\mathbf{x}_i}{dt} = \mathbf{u}(\mathbf{x}_i(t), t) + \boldsymbol{\xi}_i(t) \tag{1}$$

using the first-order Euler-Mayurama method. The velocity field $\mathbf{u}$ is tri-linearly interpolated in three-dimensional space and linearly interpolated in time using nodal values of the velocity field from lattice Boltzmann simulations stored at fixed time intervals. The molecular diffusion is modeled by $\boldsymbol{\xi}_i$ which represents uncorrelated Gaussian noise with $\langle \boldsymbol{\xi}_i \rangle = \mathbf{0}$ and is related to molecular diffusion through its variance $\left\langle \boldsymbol{\xi}_i(t)\boldsymbol{\xi}_j(t') \right\rangle = 2D_m\delta_{ij}\delta(t-t')\mathbf{1}$. Solid boundaries are handled numerically by a bounce-back-like rule: a diffusive step is only accepted if the position at the end of the time step is within a fluid phase. With this approach, a single lattice Boltzmann simulation at given flow conditions (e.g., Bo, Ca), is used as input for a range of different Pe, by running particle simulations with different molecular diffusion coefficients D_m. The method is described in more detail in Text S1 and Figure S4 in Supporting Information S1.

3. Results

In order to investigate the impact of dynamic multiphase flow on solute dispersion, we shall here consider simulations of co-flow of two immiscible fluids where the flow field is stationary. Based on our results of solute dispersion in a broad range of flow regimes, we derive a general transport law, which also offer fundamental insights into more general and transient multiphase flow systems.

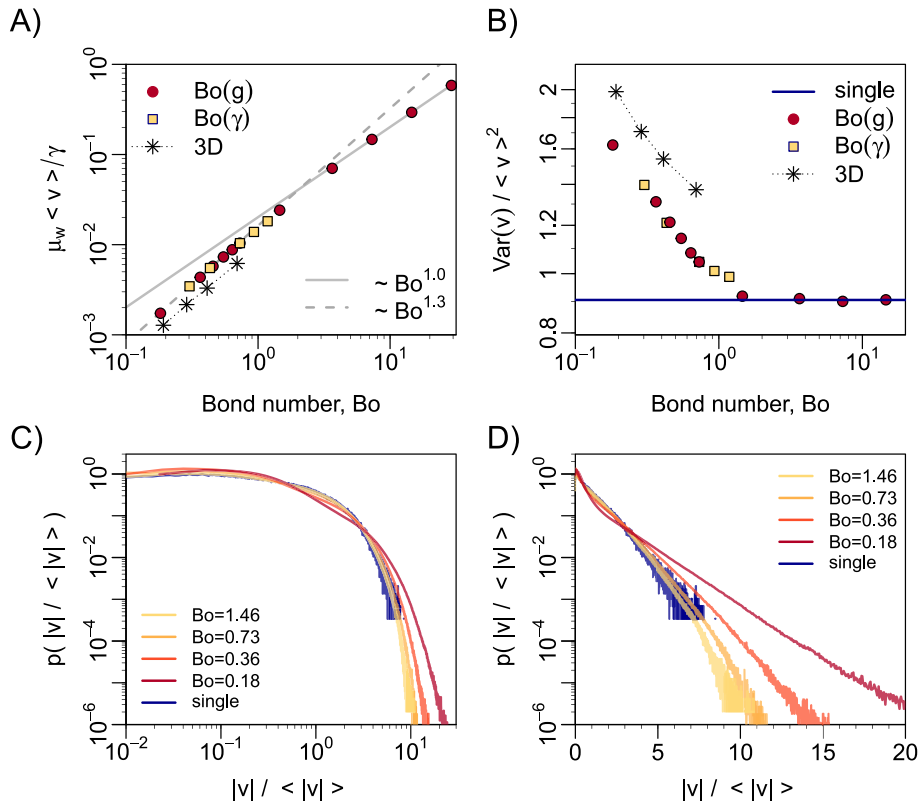

Figure 2. Characteristics of the flow field for different Bond numbers. The points marked with an * are from three-dimensional simulations, the rest are from two-dimensional simulations. (a) Non-dimensional flow rate as function of the Bond number. (b) Variance of the flow speed for different Bond numbers. (c, d) Probability density function at different Bond numbers for the velocity magnitude on respectively double and semi-logarithmic coordinates.

In our simulations, we control the driving force, which we express by the dimensionless Bond number, the ratio between the gravitational (body) force $g \equiv |\boldsymbol{g}|$ and the surface tension at the interface of the two fluid phases, $\mathrm{Bo} \equiv \ell^2 \bar{\rho} g/\gamma$, where $\bar{\rho} = (\rho_w + \rho_{nw})/2$ is the mean of the two mass densities. In our two-dimensional system, the dimensionless characteristic length scale, $\ell = 8.2$, is the average pore size between neighboring obstacles and is calculated by Voronoi tessellation. In three dimensions, we use the same scale as an approximation. We describe the flow rate by the Capillary number $\mathrm{Ca} \equiv \mu_w \langle v \rangle/\gamma$ using the dynamic viscosity of the wetting fluid μ_w. For simplicity, and without lack of generality, we take the average of the flow speed over both phases. Alternatively we could define a Capillary number specific to each phase (see Figure S3 in Supporting Information S1).

To test the generality of our findings, we have followed two simulation protocols of varying the Bond number: one where we vary the body force and hold the surface tension fixed, Bo(g), and one where the surface tension is varied and the body force is held constant, Bo(γ). Overall, our simulations are performed for Bond numbers in the range 0.1–30 and with resulting Capillary numbers in the range 10^{-4}–10. This corresponds to a dynamic fluid connectivity regime where both phases are mobile, as observed in several experiments in bead packs and rocks in the range $\mathrm{Ca} \geq 10^{-7}$ (Gao et al., 2021; Reynolds et al., 2017; Tallakstad et al., 2009a). In Figure S3 in Supporting Information S1, we confirm the persistence of dynamic fluid connectivity down to $\mathrm{Ca} \approx 10^{-4}$ from an additional set of simulations in a larger system. Whereas we focus on the two-dimensional system, we present results from a three-dimensional system to confirm the generality of our findings.

For large Bond numbers (Bo > 1), the average flow rate is proportional to the applied gravitational force, following the Darcy regime. For small Bond numbers (Bo < 1), the flow is significantly influenced by surface tension forces and crosses over to a non-Darcian behavior where $\langle v \rangle \propto \mathrm{Bo}^{\beta}$ with $\beta = 1.31$, both in 2D and 3D (Figure 2a) and consistent with experimental observations (Chevalier et al., 2015; Tallakstad et al., 2009a; Zhang et al., 2021). For large Bond numbers, the velocity probability density function is close to that of the single-phase and follows closely an exponential distribution (Figure 2d), driven by the random redistributions at pore junctions

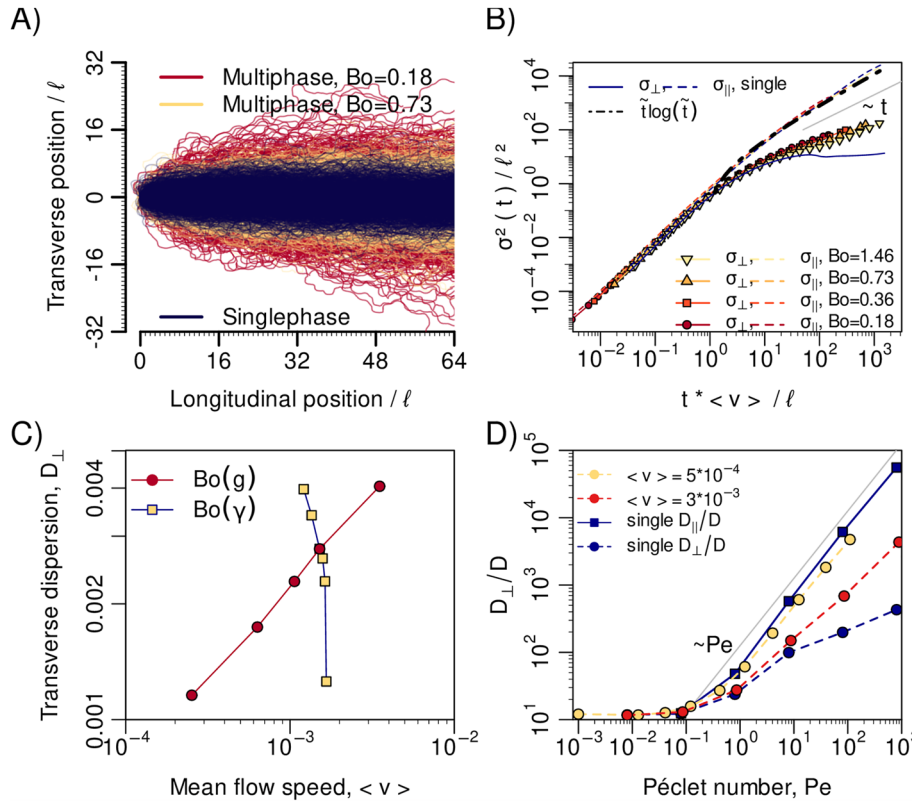

Figure 3. Panel (a) shows individual trajectories in two-dimensional simulations of passive tracers injected in three different flows, one multiphase flow at low speed (red, Bo = 0.18), one at higher speed (yellow, Bo = 0.73), and a single-phase flow (blue). All the trajectories have been shifted so they start at the center of coordinates. For each of the three flows, we plot 1,000 randomly selected trajectories. Panel (b) shows the temporal evolution of longitudinal (||) and transverse (⊥) spatial variances for two-dimensional single- and multi-phase flows with different Bond numbers using double logarithmic scales. The dashed lines represent the longitudinal particle dispersion along the flow direction. The solid lines with symbols represent the transverse dispersion. Colors yellow to red show four different Bond numbers. The blue curves are computed from a single-phase flow simulation and have a vanishing dispersion in the transverse direction. Panel (c) shows the transverse dispersion coefficient computed from Equation 2 as a function of average flow speed for the two cases where the body force, Bo(g), respectively the surface tension, Bo(γ), are varied. Panel (d) shows dispersion relative to molecular diffusion over a large range of Péclet numbers for two different flow rates.

(Alim et al., 2017). For small Bond numbers, we observe a broadening of the velocity distributions, which in the range of intermediate velocities become more power-law-like. This leads to an increase of the flow velocity variance relative to the mean velocity, following a similar behavior in two and three dimensions (Figure 2b). All the distributions are characterized by a marked exponential cutoff at large values and a plateau at low values (Figures 2c and 2d).

In order to quantify the dispersion in the fluid flow, we consider tracers over a large range of Péclet numbers $\mathrm{Pe} = \ell\langle v\rangle / D_m$ by varying D_m in Equation 1. In general, the dispersion resulting from the fluid flow becomes orders of magnitude larger than the pure molecular diffusion in the fluid. In the infinite Péclet regime Pe^{∞}, the particles follow the flow and are subject to fluctuations through spatio-temporal heterogeneity of the flow velocity field. In the simulations, the flow evolves through a transient stage and then reaches a stationary regime (when the mean and the second moment of the flow rate reach a plateau) where we start to collect the statistics of dispersion. In Figure 3a, we show the $\mathrm{Pe} = 10^6$ (diffusion effectively zero) particle trajectories for a single-phase and two multiphase simulations in two dimensions. As the Bond number is lowered, the velocity fluctuations grow relative to the mean flow and lead to particle paths that look more jagged and wander further transversely, producing an enhanced dispersion compared to single phase flow. In the following, we compute the particle dispersion from the spatial variance of the position of passive tracers.

In Figure 3b, we plot the diagonal components of the position variance tensor of the individual tracer positions x^k as function of time for $\mathrm{Pe} = 10^6$ (asymptotically close to $\mathrm{Pe}\infty$ for the time scales considered here) and for

different Bond numbers, $\boldsymbol{\sigma}^2(\Delta\tau) = \langle \left[\mathbf{x}^k(\Delta\tau + t) - \mathbf{x}^k(t)\right]\left[\mathbf{x}^k(\Delta\tau + t) - \mathbf{x}^k(t)\right]^T \rangle_{k,t}$. The average is performed over the ensemble of particles and over time. We denote the diagonal components of the position variance tensor by $\sigma_\perp^2$ and $\sigma_\parallel^2$ in the transverse and longitudinal directions, respectively (in three-dimensions we use $\sigma_\perp^2 = \sigma_{\perp,1}^2 + \sigma_{\perp,2}^2$). The longitudinal dispersion behaves similarly to that of a single-phase flow, which is apparent from Figure 3b where the longitudinal variances for multiphase flow for different Bond numbers all collapse on the single-phase flow when normalizing time by the mean velocity. The spatial variance shows a transition from the ballistic regime $\sigma_\parallel^2(t) \sim t^2$, that develops below the characteristic advection time $\tau_a = \ell/\langle v \rangle$, to a slightly super-linear growth. The broadly distributed velocity distributions together with the almost uniform velocity distribution at low velocities (Figures 2c and 2d), result in a non-Fickian longitudinal dispersion (Dentz et al., 2016) given by $\sigma_\parallel^2(t) \overset{t>\tau_a}{\approx} (t/\tau_a)\ln(t/\tau_a)$. The asymptotic scaling is verified in Figure 3b, for times larger than the characteristic advection time τ_a. As discussed in the following, the addition of diffusion induces a transition to Fickian dispersion in the longitudinal direction after a time corresponding to the time needed to diffuse a distance of the characteristic velocity correlation length (pore size for single-phase flow and fluid cluster size for multiphase flow). We note that in multiphase flow systems composed of water and air, with much larger viscosity and density ratios, the emergence of trapped clusters and dead end zones can lead to broader velocity distributions and strongly anomalous transport (Velásquez-Parra et al., 2022).

In contrast to the longitudinal behavior, the late time evolution of the transverse dispersion is Fickian, $\sigma^2 \sim t$, even for Pe^∞ (Figure 3b). The transverse dispersion varies with the flow rate and is distinctly different from the vanishing dispersion of two-dimensional single-phase flows at Pe^∞. In two-dimensional single-phase flow, the trajectories of advective particles cannot cross each other and meander over a fixed lateral distance set by the pore size. This leads to a variance asymptotically constant and a vanishing dispersion coefficient at Pe^∞. In the dynamic fluid connectivity regime, fluctuations of the flow field permit particle trajectories to cross even in the absence of diffusion. This results in continued growth of the spatial variance over time. Since the transverse dispersion is Fickian, the dispersion coefficient follows from the asymptotic behavior of $\sigma_\perp^2$,

$$D_\perp = \lim_{\Delta\tau\to\infty}\left(\frac{\sigma_\perp^2(\Delta\tau)}{2\Delta\tau}\right). \tag{2}$$

In Figure 3c, we plot the transverse dispersion computed using Equation 2 as function of the mean flow speed for Pe^∞. The dispersion behaves differently when we vary the force driving the flow in comparison to when we vary the surface tension. In the latter case, we observe that an increase in surface tension enlarges the amplitude of the transverse motion by a factor of about 4 while only moderately changing the overall flow speed. In contrast, when we vary the driving force, a similar change in dispersion requires a variation of the mean velocity over an order of magnitude. This fundamental observation tells us that the Bond number is not the right dimensionless number to characterize the dispersion, we need to identify another dimensionless number. In the following we derive a new expression for describing dispersion in the presence of dynamics connectivity.

For the persistent random walks performed by the passive tracers in the transverse direction (Masoliver & Lindenberg, 2017), the dispersion coefficient follows from the velocity correlation length, which we assume to be proportional to the typical width of fluid clusters l_c and the correlation time τ,

$$D_\perp \propto l_c^2/\tau = l_c\langle v \rangle, \tag{3}$$

with $\tau = l_c/\langle v \rangle$.

As seen from simulations (see Movie S1), the size of wetting phase clusters, l_c, is limited by fragmentation due to localized drainage. We hypothesize that, for a given l_c, the probability of fluid cluster fragmentation depends on the probability that the cluster perimeter includes pores whose threshold capillary pressure for drainage is larger than the average pressure jumps across the cluster $\Delta p = l_c\rho g$. We further assume that the distribution of threshold capillary pressures for drainage follows an exponential distribution, $p(p_c) = \eta^{-1}e^{-p_c/\eta}$. The average threshold capillary pressure $\eta \propto \gamma/\ell$ is proportional to the surface tension divided by a characteristic length scale for a fluid interface moving through a pore throat, which again is proportional to the typical pore size ℓ. The probability that the pressure difference in a given pore on the cluster perimeter is less than the threshold is $q = e^{-\Delta p/\eta}$. Hence, the probability that all pores on the cluster perimeters are below the threshold is q^n, with $n \sim l_c/\ell$. The probability to maintain a cluster of size l_c is therefore $p(l_c) \sim \exp\left[-l_c^2\rho g/(\eta\ell)\right] = \exp\left[-l_c^2\rho g/\gamma\right]$, which leads to an average cluster size,

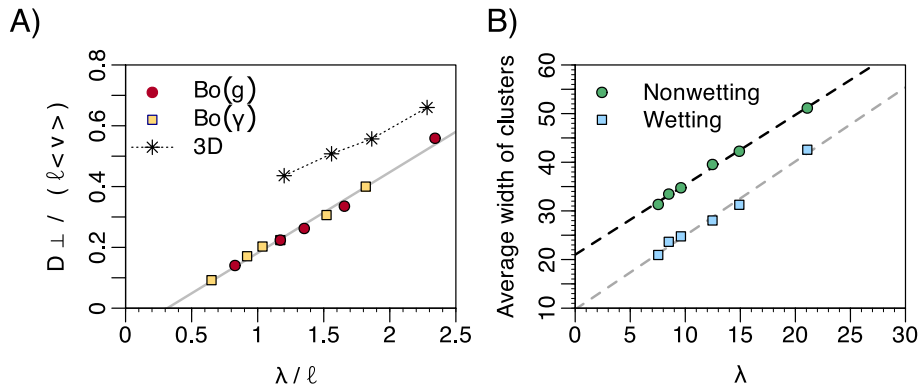

Figure 4. (a) Transverse dispersion as a function of the effective length scale λ. The gray line is a best linear fit (slope = 0.26 ± 0.02). Data from three-dimensional simulations are marked by an *. (b) Average transverse width of fluid clusters in the 2D simulations as a function of λ for respectively the wetting (blue squares) and the non-wetting phases (green circles). The gray lines are best linear fits to the points with a slope = 1.5 ± 0.1 for the wetting clusters and a slope = 1.4 ± 0.1 for the non-wetting clusters.

$$\langle l_c \rangle \sim \lambda \equiv \sqrt{\frac{\gamma}{\rho g}}. \tag{4}$$

Interestingly, we recover the classical capillary length, usually derived for a free droplet. We note that this result is not the consequence of a standard dimensional analysis, but follows from statistical considerations. In Figure 4b, we plot the average width of clusters (measured as the transverse spatial extent) as function of λ, which confirms Equation 4. Note that the theory presented here may be generalized to cluster sizes that can develop in other multiphase flow regimes, with much larger viscosity or density ratios (Tallakstad et al., 2009a, 2009b).

Inserting Equation 4 in Equation 3, we obtain as a key result here, a relation for the transverse solute dispersion

$$D_\perp \propto \lambda \langle v \rangle = \frac{\ell \langle v \rangle}{\sqrt{\mathrm{Bo}}}, \tag{5}$$

which is confirmed by the data-collapse in Figure 4a of the data displayed in Figure 3c. Note that this data collapse shows that rather than the Bond and Capillary numbers, the most simple dimensionless number characterizing dispersion is the fluid cluster size scaled with pore scale. Our result also holds in three-dimensions but with a larger pre-factor due to larger transverse dispersion (Figure 4a).

In addition to the large Pe regime, we have investigated the effect of diffusion on dispersion in multiphase flows over a large range of Péclet numbers, $10^{-3} \leq \mathrm{Pe} \leq 10^3$ (Figure 3d). For any finite Péclet number, longitudinal dispersion becomes asymptotically Fickian as diffusion introduces a cut-off time in the travel time distribution (Bijeljic et al., 2011; Puyguiraud et al., 2021). The longitudinal dispersion coefficient follows the classical transition from $D_\parallel = D_m$ for Pe < 1 to $D_\parallel \sim \mathrm{Pe}$ for Pe > 1 (Dentz et al., 2011). In single phase flow, transverse dispersion is much smaller than longitudinal dispersion for moderate to high Péclet numbers, as usually assumed in transport models (Dentz et al., 2011). In contrast, dynamic fluid connectivity in multiphase flows significantly increases transverse dispersion, which can reach a similar amplitude as longitudinal dispersion for low Capillary numbers. At Bo = 0.73, the enhancement of transverse dispersion compared to the single phase case in two-dimensions is thus a factor 8 for Pe = 10 and a factor 50 for Pe = 100 (Figure 3d).

Whereas dispersion is classically described to be a function of the Péclet number (Bijeljic et al., 2011; Dagan, 1984; Dentz et al., 2011; Gelhar & Axness, 1983), our results show that it can vary largely for any given Péclet number depending on the multiphase flow properties (Figure 3d). In single phase systems, the dispersion versus Péclet function is uniquely related to the pore structure (Puyguiraud et al., 2021). Therefore, we emphasize that dispersion must be considered in the combined Péclet number—Capillary number space, consistent with our theoretical prediction (Equation 5). For Pe < 1, solute dispersion is diffusion dominated and we observe little to no difference between single and multiphase flows (Figure 5a). For lower Capillary numbers, the dynamic fluid connectivity controls dispersion, which is greatly amplified relative to single phase flow. Whereas, we only

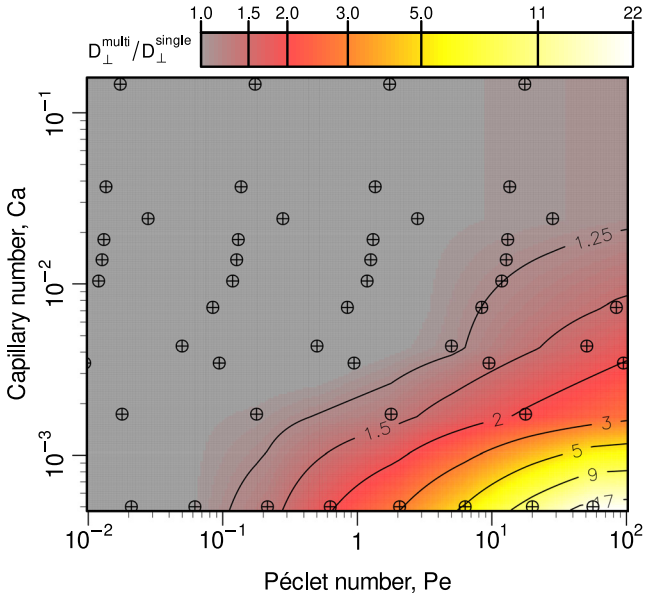

Figure 5. Phase diagram of the transverse dispersion dynamics in the Capillary number versus Péclet number space. The color scale indicates the ratio between the dispersion coefficient $D_\perp^{multi}$ in the multiphase flow relative to corresponding coefficient for a single phase flow $D_\perp^{single}$. The black lines show a few level curves. In the larger Ca number and low Pe number region (gray), the dispersion is diffusion dominated and $D_\perp^{multi}/D_\perp^{single} \sim 1$. In the colored region, the dispersion of the multiphase flow is greatly amplified by the dynamic connectivity and can for the Péclet numbers considered be amplified by more than an order magnitude relative to single phase flow. The data points used to generate the plot are marked by "⊕."

observe an increase in dispersion as we lower the Capillary numbers, there might be a lower critical value (likely system size dependent) where capillary forces dominate the viscous forces to an extent that the distribution of fluid phases is frozen (Gao et al., 2021). In this regime and depending on the boundary conditions, the two phases can flow in parallel (Datta et al., 2014) or one phase flows around a trapped phase (Jiménez-Martínez et al., 2015). For different porous media structures, the transition has been found to vary between 10^{-7} and 10^{-4} (Gao et al., 2021). When viscous forces dominate over capillary forces, linear Darcy flow is recovered, which is expected to happen for Capillary numbers in the range 10^{-2}–10^{-1} (Yiotis et al., 2013), consistent with our results (Figure 2a).

While we have studied here dynamic co-flow systems under global steady-state conditions, the results are relevant for a broad range of transient multiphase flow systems where dynamic flow connectivity occurs as the saturation and flow rate evolve in space and time. Transient multiphase flows play an important role in solute transport in unsaturated soils (Vereecken et al., 2022), gas and brine flow in porous rock (Reynolds et al., 2017), CO_2 and brine flow in subsurface reservoirs (Zheng et al., 2017), water and hydrogen flow in porous media (Lysyy et al., 2022), and water and air in snow and ice (Waldner et al., 2004). A typical range of dimensionless numbers for multiphase flow in porous media systems is Ca = $\{10^{-7}$–$10^{-3}\}$ and Pe = $\{1$–$10^{2}\}$, which overlaps with the enhanced dispersion regime described here (Figure 5). This phenomenon hence likely affects the transport, mixing, and reaction of dissolved elements, such as contaminants, nutrients, CO_2, hydrogen, salts, and ions, in a broad range of natural and geoengineered systems.

4. Conclusion

Transient dynamics and flow intermittency is a key property of multiphase flow in porous media, occurring over a broad range of Capillary numbers above the threshold for mobilization of the fluid phases (Armstrong et al., 2014; Gao et al., 2021). We have shown that the repeated activation and deactivation of flow paths, dynamic connectivity, induces a large variability of the flow field, with a strong enhancement of transverse solute dispersion. While previous works have associated the enhancement of dispersion in unsaturated flows to a greater variability of velocity, we have shown here that the main driver for this phenomenon is the change of the size of water/air clusters with saturation. We have derived a fundamental scaling law for dispersion in dynamic multiphase flow in porous media emphasizing that dispersion must be described in combined Capillary number—Péclet number space. To establish these laws, we have here considered multiphase flow under global steady state conditions. However, our findings will be relevant for understanding the role of dynamic connectivity on solute transport in a broad range of transient systems, hence impacting a large range of phenomena occurring in natural and engineered porous media systems.

Future work should explore solute transport dynamics over a range of wetting contact angles, viscosities, and densities and explore the impact of transient flows. Our findings can be used to tune solute dispersion in porous media by altering the ratio between the surface forces and the force driving the flow. Strikingly, dispersion can be controlled by changing the surface tension between fluids without modifying the mean velocity. Our results also suggest that transverse dispersion could be used as a macroscopic metric for characterizing the dynamics of two-phase flows. This opens new perspectives for characterizing, modeling and controlling multiphase flow and transport processes in natural systems.

Data Availability Statement

The numerical code used to generate all the data presented in this manuscript is available at https://doi.org/10.5281/zenodo.8212058.

Acknowledgments
This study received funding from the Akademiaavtaalen between the University of Oslo and Equinor (Project MODIF-LOW to F. Renard). Joachim Mathiesen acknowledges support from the ESS lighthouse on hard materials in 3D, SOLID, funded by the Danish Agency for Science and Higher Education, Grant 8144-00002B.

References

Aiken, J. M., Sohn, R. A., Renard, F., Matter, J., Kelemen, P., & Jamtveit, B. (2022). Gas migration episodes observed during peridotite alteration in the Samail ophiolite, Oman. *Geophysical Research Letters*, *49*(21), e2022GL100395. https://doi.org/10.1029/2022gl100395

Alim, K., Parsa, S., Weitz, D. A., & Brenner, M. P. (2017). Local pore size correlations determine flow distributions in porous media. *Physical Review Letters*, *119*(14), 144501. https://doi.org/10.1103/physrevlett.119.144501

Armstrong, R. T., Georgiadis, A., Ott, H., Klemin, D., & Berg, S. (2014). Critical capillary number: Desaturation studied with fast x-ray computed microtomography. *Geophysical Research Letters*, *41*(1), 55–60. https://doi.org/10.1002/2013gl058075

Berkowitz, B., Cortis, A., Dentz, M., & Scher, H. (2006). Modeling non-Fickian transport in geological formations as a continuous time random walk. *Reviews of Geophysics*, *44*(2), RG2003. https://doi.org/10.1029/2005rg000178

Bijeljic, B., Mostaghimi, P., & Blunt, M. J. (2011). Signature of non-Fickian solute transport in complex heterogeneous porous media. *Physical Review Letters*, *107*(20), 204502. https://doi.org/10.1103/physrevlett.107.204502

Blunt, M. J. (2017). *Multiphase flow in permeable media: A pore-scale perspective*. Cambridge university press.

Bochet, O., Bethencourt, L., Dufresne, A., Farasin, J., Pédrot, M., Labasque, T., et al. (2020). Iron-oxidizer hotspots formed by intermittent oxic–anoxic fluid mixing in fractured rocks. *Nature Geoscience*, *13*(2), 149–155. https://doi.org/10.1038/s41561-019-0509-1

Bordoloi, A. D., Scheidweiler, D., Dentz, M., Bouabdellaoui, M., Abbarchi, M., & de Anna, P. (2022). Structure induced laminar vortices control anomalous dispersion in porous media. *Nature Communications*, *13*(1), 3820. https://doi.org/10.1038/s41467-022-31552-5

Bromly, M., & Hinz, C. (2004). Non-Fickian transport in homogeneous unsaturated repacked sand. *Water Resources Research*, *40*(7), W07402. https://doi.org/10.1029/2003wr002579

Chen, L., He, Y., Tao, W.-Q., Zelenay, P., Mukundan, R., & Kang, Q. (2017). Pore-scale study of multiphase reactive transport in fibrous electrodes of vanadium redox flow batteries. *Electrochimica Acta*, *248*, 425–439. https://doi.org/10.1016/j.electacta.2017.07.086

Chevalier, T., Salin, D., Talon, L., & Yiotis, A. G. (2015). History effects on nonwetting fluid residuals during desaturation flow through disordered porous media. *Physical Review E*, *91*(4), 043015. https://doi.org/10.1103/physreve.91.043015

Connington, K., & Lee, T. (2013). Lattice Boltzmann simulations of forced wetting transitions of drops on superhydrophobic surfaces. *Journal of Computational Physics*, *250*(Supplement C), 601–615. https://doi.org/10.1016/j.jcp.2013.05.012

Dagan, G. (1984). Solute transport in heterogeneous porous formations. *Journal of Fluid Mechanics*, *145*(-1), 151–177. https://doi.org/10.1017/s0022112084002858

Datta, S. S., Dupin, J.-B., & Weitz, D. A. (2014). Fluid breakup during simultaneous two-phase flow through a three-dimensional porous medium. *Physics of Fluids*, *26*(6), 062004. https://doi.org/10.1063/1.4884955

De Anna, P., Le Borgne, T., Dentz, M., Tartakovsky, A. M., Bolster, D., & Davy, P. (2013). Flow intermittency, dispersion, and correlated continuous time random walks in porous media. *Physical Review Letters*, *110*(18), 184502. https://doi.org/10.1103/physrevlett.110.184502

De Gennes, P. (1983). Hydrodynamic dispersion in unsaturated porous media. *Journal of Fluid Mechanics*, *136*(-1), 189–200. https://doi.org/10.1017/s0022112083002116

Dentz, M., Kang, P. K., Comolli, A., Le Borgne, T., & Lester, D. R. (2016). Continuous time random walks for the evolution of Lagrangian velocities. *Physical Review Fluids*, *1*(7), 074004. https://doi.org/10.1103/physrevfluids.1.074004

Dentz, M., Le Borgne, T., Englert, A., & Bijeljic, B. (2011). Mixing, spreading and reaction in heterogeneous media: A brief review. *Journal of Contaminant Hydrology*, *120*, 1–17. https://doi.org/10.1016/j.jconhyd.2010.05.002

Dougherty, A., & Carle, N. (1998). Distribution of avalanches in interfacial motion in a porous medium. *Physical Review E*, *58*(3), 2889–2893. https://doi.org/10.1103/physreve.58.2889

Ferrari, A., Jimenez-Martinez, J., Borgne, T. L., Méheust, Y., & Lunati, I. (2015). Challenges in modeling unstable two-phase flow experiments in porous micromodels. *Water Resources Research*, *51*(3), 1381–1400. https://doi.org/10.1002/2014wr016384

Gao, Y., Lin, Q., Bijeljic, B., & Blunt, M. J. (2020). Pore-scale dynamics and the multiphase Darcy law. *Physical Review Fluids*, *5*(1), 013801. https://doi.org/10.1103/physrevfluids.5.013801

Gao, Y., Raeini, A. Q., Blunt, M. J., & Bijeljic, B. (2021). Dynamic fluid configurations in steady-state two-phase flow in Bentheimer sandstone. *Physical Review E*, *103*(1), 013110. https://doi.org/10.1103/physreve.103.013110

Gelhar, L. W., & Axness, C. L. (1983). Three-dimensional stochastic analysis of macrodispersion in aquifers. *Water Resources Research*, *19*(1), 161–180. https://doi.org/10.1029/wr019i001p00161

Golden, K. (2001). Brine percolation and the transport properties of sea ice. *Annals of Glaciology*, *33*, 28–36. https://doi.org/10.3189/172756401781818329

Harter, T., & Yeh, T.-C. J. (1996). Conditional stochastic analysis of solute transport in heterogeneous, variably saturated soils. *Water Resources Research*, *32*(6), 1597–1609. https://doi.org/10.1029/96wr00503

Hartmann, A., Jasechko, S., Gleeson, T., Wada, Y., Andreo, B., Barberá, J. A., et al. (2021). Risk of groundwater contamination widely underestimated because of fast flow into aquifers. *Proceedings of the National Academy of Sciences of the United States of America*, *118*(20), e2024492118. https://doi.org/10.1073/pnas.2024492118

Harvey, C. F., Swartz, C. H., Badruzzaman, A., Keon-Blute, N., Yu, W., Ali, M. A., et al. (2002). Arsenic mobility and groundwater extraction in Bangladesh. *Science*, *298*(5598), 1602–1606. https://doi.org/10.1126/science.1076978

Hasan, S., Niasar, V., Karadimitriou, N. K., Godinho, J. R., Vo, N. T., An, S., et al. (2020). Direct characterization of solute transport in unsaturated porous media using fast x-ray synchrotron microtomography. *Proceedings of the National Academy of Sciences of the United States of America*, *117*(38), 23443–23449. https://doi.org/10.1073/pnas.2011716117

Holtzman, R., Dentz, M., Planet, R., & Ortín, J. (2020). The origin of hysteresis and memory of two-phase flow in disordered media. *Communications Physics*, *3*(1), 222. https://doi.org/10.1038/s42005-020-00492-1

Jiménez-Martínez, J., Anna, P. D., Tabuteau, H., Turuban, R., Borgne, T. L., & Méheust, Y. (2015). Pore-scale mechanisms for the enhancement of mixing in unsaturated porous media and implications for chemical reactions. *Geophysical Research Letters*, *42*(13), 5316–5324. https://doi.org/10.1002/2015gl064513

Jiménez-Martínez, J., Le Borgne, T., Tabuteau, H., & Méheust, Y. (2017). Impact of saturation on dispersion and mixing in porous media: Photobleaching pulse injection experiments and shear-enhanced mixing model. *Water Resources Research*, *53*(2), 1457–1472. https://doi.org/10.1002/2016wr019849

Kang, P. K., Anna, P., Nunes, J. P., Bijeljic, B., Blunt, M. J., & Juanes, R. (2014). Pore-scale intermittent velocity structure underpinning anomalous transport through 3-D porous media. *Geophysical Research Letters*, *41*(17), 6184–6190. https://doi.org/10.1002/2014gl061475

Kirchner, J. W., Feng, X., & Neal, C. (2000). Fractal stream chemistry and its implications for contaminant transport in catchments. *Nature*, *403*(6769), 524–527. https://doi.org/10.1038/35000537

Le Borgne, T., Dentz, M., & Carrera, J. (2008). Lagrangian statistical model for transport in highly heterogeneous velocity fields. *Physical Review Letters*, *101*(9), 090601. https://doi.org/10.1103/physrevlett.101.090601

Lysyy, M., Ersland, G., & Fernø, M. (2022). Pore-scale dynamics for underground porous media hydrogen storage. *Advances in Water Resources*, *163*, 104167. https://doi.org/10.1016/j.advwatres.2022.104167

Masoliver, J., & Lindenberg, K. (2017). Continuous time persistent random walk: A review and some generalizations. *The European Physical Journal B*, *90*(6), 1–13. https://doi.org/10.1140/epjb/e2017-80123-7

Mathiesen, J., Linga, G., Misztal, M., Borgne, T. L., & Renard, F. (2023). Software for simulating solute dispersion in multiphase porous media flow. *Zenodo*. https://doi.org/10.5281/zenodo.8212058

Meigel, F. J., Darwent, T., Bastin, L., Goehring, L., & Alim, K. (2022). Dispersive transport dynamics in porous media emerge from local correlations. *Nature Communications*, *13*(1), 1–9. https://doi.org/10.1038/s41467-022-33485-5

Neuman, S. P., & Tartakovsky, D. M. (2009). Perspective on theories of non-Fickian transport in heterogeneous media. *Advances in Water Resources*, *32*(5), 670–680. https://doi.org/10.1016/j.advwatres.2008.08.005

Nützmann, G., Maciejewski, S., & Joswig, K. (2002). Estimation of water saturation dependence of dispersion in unsaturated porous media: Experiments and modelling analysis. *Advances in Water Resources*, *25*(5), 565–576. https://doi.org/10.1016/s0309-1708(02)00018-0

Osselin, F., Soulaine, C., Fauguerolles, C., Gaucher, E., Scaillet, B., & Pichavant, M. (2022). Orange hydrogen is the new green. *Nature Geoscience*, *15*(10), 765–769. https://doi.org/10.1038/s41561-022-01043-9

Padilla, I. Y., Yeh, T.-C. J., & Conklin, M. H. (1999). The effect of water content on solute transport in unsaturated porous media. *Water Resources Research*, *35*(11), 3303–3313. https://doi.org/10.1029/1999wr900171

Planet, R., Santucci, S., & Ortín, J. (2009). Avalanches and non-Gaussian fluctuations of the global velocity of imbibition fronts. *Physical Review Letters*, *102*(9), 094502. https://doi.org/10.1103/physrevlett.102.094502

Primkulov, B. K., Zhao, B., MacMinn, C. W., & Juanes, R. (2022). Avalanches in strong imbibition. *Communications Physics*, *5*(1), 52. https://doi.org/10.1038/s42005-022-00826-1

Puyguiraud, A., Gouze, P., & Dentz, M. (2021). Pore-scale mixing and the evolution of hydrodynamic dispersion in porous media. *Physical Review Letters*, *126*(16), 164501. https://doi.org/10.1103/physrevlett.126.164501

Ramstad, T., Idowu, N., Nardi, C., & Øren, P.-E. (2012). Relative permeability calculations from two-phase flow simulations directly on digital images of porous rocks. *Transport in Porous Media*, *94*(2), 487–504. https://doi.org/10.1007/s11242-011-9877-8

Reynolds, C. A., Menke, H., Andrew, M., Blunt, M. J., & Krevor, S. (2017). Dynamic fluid connectivity during steady-state multiphase flow in a sandstone. *Proceedings of the National Academy of Sciences of the United States of America*, *114*(31), 8187–8192. https://doi.org/10.1073/pnas.1702834114

Rolle, M., & Le Borgne, T. (2019). Mixing and reactive fronts in the subsurface. *Reviews in Mineralogy and Geochemistry*, *85*(1), 111–142. https://doi.org/10.2138/rmg.2018.85.5

Rücker, M., Berg, S., Armstrong, R., Georgiadis, A., Ott, H., Schwing, A., et al. (2015). From connected pathway flow to ganglion dynamics. *Geophysical Research Letters*, *42*(10), 3888–3894. https://doi.org/10.1002/2015gl064007

Scandella, B. P., Pillsbury, L., Weber, T., Ruppel, C., Hemond, H. F., & Juanes, R. (2016). Ephemerality of discrete methane vents in lake sediments. *Geophysical Research Letters*, *43*(9), 4374–4381. https://doi.org/10.1002/2016gl068668

Sebilo, M., Mayer, B., Nicolardot, B., Pinay, G., & Mariotti, A. (2013). Long-term fate of nitrate fertilizer in agricultural soils. *Proceedings of the National Academy of Sciences of the United States of America*, *110*(45), 18185–18189. https://doi.org/10.1073/pnas.1305372110

Szulczewski, M. L., MacMinn, C. W., Herzog, H. J., & Juanes, R. (2012). Lifetime of carbon capture and storage as a climate-change mitigation technology. *Proceedings of the National Academy of Sciences of the United States of America*, *109*(14), 5185–5189. https://doi.org/10.1073/pnas.1115347109

Tallakstad, K. T., Knudsen, H. A., Ramstad, T., Løvoll, G., Måløy, K. J., Toussaint, R., & Flekkøy, E. G. (2009a). Steady-state two-phase flow in porous media: Statistics and transport properties. *Physical Review Letters*, *102*(7), 074502. https://doi.org/10.1103/physrevlett.102.074502

Tallakstad, K. T., Løvoll, G., Knudsen, H. A., Ramstad, T., Flekkøy, E. G., & Måløy, K. J. (2009b). Steady-state, simultaneous two-phase flow in porous media: An experimental study. *Physical Review E*, *80*(3), 036308. https://doi.org/10.1103/physreve.80.036308

Tarkowski, R. (2019). Underground hydrogen storage: Characteristics and prospects. *Renewable and Sustainable Energy Reviews*, *105*, 86–94. https://doi.org/10.1016/j.rser.2019.01.051

Triadis, D., Jiang, F., & Bolster, D. (2019). Anomalous dispersion in pore-scale simulations of two-phase flow. *Transport in Porous Media*, *126*(2), 337–353. https://doi.org/10.1007/s11242-018-1155-6

Vanderborght, J., & Vereecken, H. (2007). Review of dispersivities for transport modeling in soils. *Vadose Zone Journal*, *6*(1), 29–52. https://doi.org/10.2136/vzj2006.0096

Velásquez-Parra, A., Aquino, T., Willmann, M., Méheust, Y., Le Borgne, T., & Jiménez-Martínez, J. (2022). Sharp transition to strongly anomalous transport in unsaturated porous media. *Geophysical Research Letters*, *49*(3), e2021GL096280. https://doi.org/10.1029/2021gl096280

Vereecken, H., Amelung, W., Bauke, S. L., Bogena, H., Brüggemann, N., Montzka, C., et al. (2022). Soil hydrology in the Earth system. *Nature Reviews Earth & Environment*, *3*(9), 573–587. https://doi.org/10.1038/s43017-022-00324-6

Waldner, P. A., Schneebeli, M., Schultze-Zimmermann, U., & Flühler, H. (2004). Effect of snow structure on water flow and solute transport. *Hydrological Processes*, *18*(7), 1271–1290. https://doi.org/10.1002/hyp.1401

Yeh, T.-C. J., Dong, Y., & Ye, S. (2023). *An introduction to solute transport in heterogeneous geologic media*. Cambridge University Press.

Yiotis, A., Talon, L., & Salin, D. (2013). Blob population dynamics during immiscible two-phase flows in reconstructed porous media. *Physical Review E*, *87*(3), 033001. https://doi.org/10.1103/physreve.87.033001

Zhang, Y., Bijeljic, B., Gao, Y., Lin, Q., & Blunt, M. J. (2021). Quantification of nonlinear multiphase flow in porous media. *Geophysical Research Letters*, *48*(5), e2020GL090477. https://doi.org/10.1029/2020gl090477

Zhao, B., MacMinn, C. W., & Juanes, R. (2016). Wettability control on multiphase flow in patterned microfluidics. *Proceedings of the National Academy of Sciences of the United States of America*, *113*(37), 10251–10256. https://doi.org/10.1073/pnas.1603387113

Zheng, X., Mahabadi, N., Yun, T. S., & Jang, J. (2017). Effect of capillary and viscous force on CO_2 saturation and invasion pattern in the microfluidic chip. *Journal of Geophysical Research: Solid Earth*, *122*(3), 1634–1647. https://doi.org/10.1002/2016jb013908

References From the Supporting Information

Aris, R. (1956). On the dispersion of a solute in a fluid flowing through a tube. *Proceedings of the Royal Society of London. Series A. Mathematical and Physical Sciences*, *235*(1200), 67–77.

d'Humières, D., & Ginzburg, I. (2009). Viscosity independent numerical errors for lattice Boltzmann models: From recurrence equations to "magic" collision numbers. *Computers & Mathematics with Applications*, *58*(5), 823–840. https://doi.org/10.1016/j.camwa.2009.02.008

d'Humières, D., Ginzburg, I., Krafczyk, M., Lallemand, P., & Luo, L.-S. (2002). Multiple-relaxation-time lattice Boltzmann models in three dimensions. *Philosophical Transactions of the Royal Society of London. Series A: Mathematical, Physical and Engineering Sciences*, *360*, 437–451. https://doi.org/10.1098/rsta.2001.0955

Fakhari, A., & Lee, T. (2013). Multiple-relaxation-time lattice Boltzmann method for immiscible fluids at high Reynolds numbers. *Physical Review E - Statistical Physics, Plasmas, Fluids, and Related Interdisciplinary Topics*, *87*(2), 023304. https://doi.org/10.1103/PhysRevE.87.023304

Lee, T., & Liu, L. (2010). Lattice Boltzmann simulations of micron-scale drop impact on dry surfaces. *Journal of Computational Physics*, *229*(20), 8045–8063. https://doi.org/10.1016/j.jcp.2010.07.007

Nash, R. W., Carver, H. B., Bernabeu, M. O., Hetherington, J., Groen, D., Krüger, T., & Coveney, P. V. (2014). Choice of boundary condition for lattice-Boltzmann simulation of moderate-Reynolds-number flow in complex domains. *Physical Review E*, *89*(2), 023303. https://doi.org/10.1103/PhysRevE.89.023303

Taylor, G. I. (1953). Dispersion of soluble matter in solvent flowing slowly through a tube. *Proceedings of the Royal Society of London. Series A. Mathematical and Physical Sciences*, *219*(1137), 186–203.

Ziegler, D. P. (1993). Boundary conditions for lattice Boltzmann simulations. *Journal of Statistical Physics*, *71*(5), 1171–1177. https://doi.org/10.1007/BF01049965